Journal of Alloys and Compounds 509S (2011) S719–S723

Contents lists available at ScienceDirect

Journal of Alloys and Compounds

journal homepage: www.elsevier.com/locate/jallcom

Hydrogen release and structural transformations in $LiNH_2$–MgH_2 systems

D. Pottmaier[a], F. Dolci[b], M. Orlova[c], G. Vaughan[c], M. Fichtner[d], W. Lohstroh[d], M. Baricco[a,*]

[a] Dipartimento di Chimica IFM and NIS, Università di Torino – Turin, Italy
[b] Institute for Energy DG, Joint Research Center – Petten, Netherlands
[c] ID11, European Synchrotron Radiation Facility – Grenoble, France
[d] Institute of Nanotechnology, Karlsruhe Institute of Technology – Karlsruhe, Germany

ARTICLE INFO

Article history:
Received 15 August 2010
Received in revised form 11 October 2010
Accepted 27 October 2010
Available online 4 November 2010

Keywords:
Lithium amide
Magnesium hydride
Hydrogen storage
Thermal programmed desorption
Differential scanning calorimetry
In situ synchrotron X-ray diffraction

ABSTRACT

Reactive hydride composites are good candidates for solid hydrogen storage due to their high gravimetric capacity, cyclability, and suitable thermodynamic properties. The $LiNH_2$–MgH_2 system is promising as changes in stoichiometry and milling conditions may result in tailoring of these properties. In this work, $LiNH_2$–MgH_2 with different ratios (Li2:Mg, Li:Mg) and ball milling conditions (100, 600 rpm) were investigated. Thermal desorption profiles shows hydrogen release starting at 125 °C for Li2:Mg 600 sample and at 225 °C for Li:Mg 600 sample, while for Li:Mg 100 sample simultaneous hydrogen and ammonia release at 175 °C is observed. In-situ synchrotron X-ray diffraction shows the related structural transformations, such as formation of $Mg(NH_2)_2$ and allotropic transformation of α into β-$Li_2Mg(NH)_2$ for Li2:Mg 600 sample at 350 °C or direct formation of β-$Li_2Mg(NH)_2$ for Li:Mg 100 sample at 370 °C. Different polymorphs of the LiMgN phase were also observed during cooling for these two samples. For the Li:Mg 600 sample, transformation occurs in a unique reaction from an unknown phase into β-$Li_2Mg(NH)_2$ at 290 °C. The unknown phase is indexed as a *Fm*3*m* cubic similar to the high temperature γ-$Li_2Mg(NH)_2$.

1. Introduction

Reactive hydride composites, obtained by ball milling a metal hydride (A-H, A = Li, Na, Mg, ...) and a complex hydride (A-X-H, X = N, B, Al), have been subject of intense investigation for solid state hydrogen storage. The amide/hydride system was brought to the hydrogen storage field by the pioneer work of Chen et al. [1], demonstrating the suitable sorption reactions of the $LiNH_2$:2LiH composite. Such materials are very attractive for solid state hydrogen storage due to their high storage capacity, good cyclability and good thermodynamic properties [1–8]. The search for means to destabilize $LiNH_2$ leads to the partial substitution of Li by Mg using different approaches [2–5] and the corresponding change in the enthalpy amounts from about 60 KJ/mol H_2 for $LiNH_2$:LiH to about 30 KJ/mol H_2 for $2LiNH_2$:MgH_2 [6]. In agreement with different studies [2,3], the hydrogen exchange reaction of the $2LiNH_2$:MgH_2 system (Li2:Mg), passing or not by metathesis reactions already during ball milling, can be written as:

$$2LiNH_2 + MgH_2 \rightarrow Li_2Mg(NH)_2 + 2H_2 \leftrightarrow Mg(NH_2)_2 + 2LiH \quad (1)$$

On the other hand, fewer studies were performed in the $LiNH_2$:MgH_2 system (Li:Mg) and some controversy exists among theoretical approaches [6,7] suggesting the reaction

$$LiNH_2 + MgH_2 \leftrightarrow LiMgN + 2H_2 \quad (2)$$

and experimental results [9,10], which observed different desorption reactions:

$$LiNH_2 + MgH_2 \rightarrow 1/3Mg_3N_2 + 3LiH + 1/3Li_2Mg_2(NH)_3 + 3/2H_2 \quad (3)$$

$$LiNH_2 + MgH_2 \rightarrow 1/4Mg_3N_2 + 1/4LiH + 1/4Li_2Mg(NH)_2 + 3/2H_2 \quad (4)$$

The system $LiNH_2$–MgH_2 is a promising one, as changes in stoichiometry [11–15] and ball milling conditions [16–19] result in different reaction mechanisms. One expects the former to change the reaction pathway by tailoring thermodynamics and the second to interfere in the kinetics aspects. However, what is observed always in experiments is an interplay of the two effects. In the present work, we analyze both the difference in stoichiometry, considering Li2:Mg and Li:Mg composites, and ball milling preparation, using a rotation speed of 100 and 600 rpm. The desorption behavior and corresponding structural phase transformations of these samples will be discussed.

* Corresponding author. Tel.: +39 011 6707569; fax: +39 011 6707855.
E-mail address: marcello.baricco@unito.it (M. Baricco).

0925-8388/$ – see front matter © 2010 Elsevier B.V. All rights reserved.
doi:10.1016/j.jallcom.2010.10.166

2. Experimental

Starting materials, $LiNH_2$ (99%) and MgH_2 (95%), were purchased from Sigma Aldrich and used as received without any further purification. Composite samples were prepared by ball milling in different ratios of Li:Mg using a Fritsch P6 planetary equipment with vial and balls of silicon nitride, under an argon atmosphere, for 12 h each, and a powder to ball ratio of 1:20. Milling rotation speeds of 100 and 600 rpm were used. Mass spectroscopy (MS) was performed using a quadropole mass spectrometer (Catlab Hiden) with a helium flow of 50 mL/min for identification of gaseous species. Thermal programmed desorption (TPD) was performed with a volumetric instrument (Advanced Materials) under initial static vacuum of 10^{-4} mbar for hydrogen release quantification. High pressure differential scanning

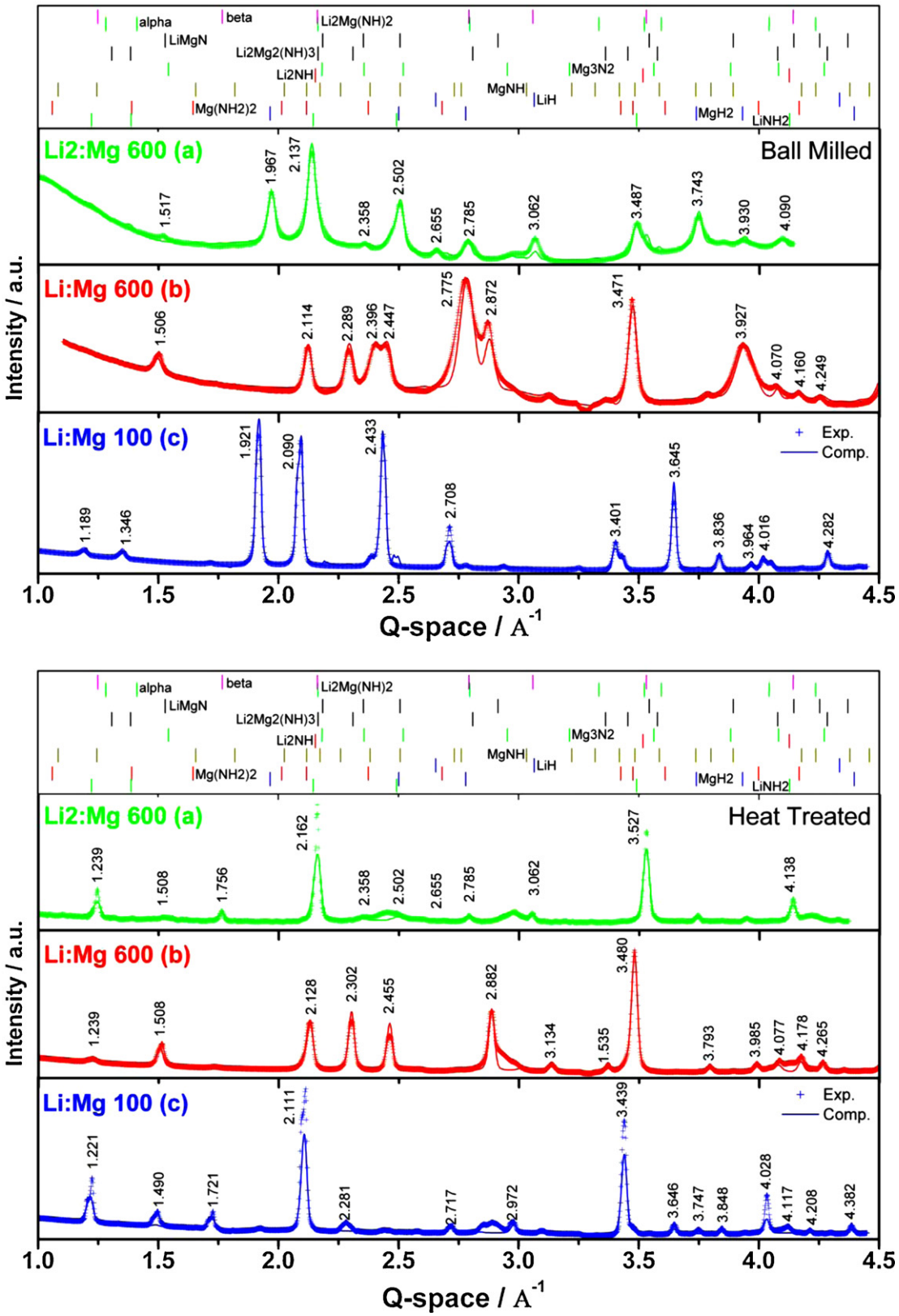

Fig. 1. SXRD patterns at room temperature top and bottom heat treatment of samples: Li2:Mg 600 (a), Li:Mg 600 (b), and Li:Mg 100 (c). Symbols: experimental points; lines: calculated from Rietveld refinement.

calorimetry (DSC) was performed under a static pressure of 3 atm helium (Netzsch HP 204 Phoenix) for reactions nature analysis. All three thermal analysis (MS, TPD, DSC) were conducted in continuous mode up to 400 °C at a heating rate of 10 °C/min. In-situ synchrotron X-ray diffraction (SXRD) data were collected with an energy of 42 keV ($\lambda = 0.2952$ Å), with an exposure time of 60 s using an image plate detector. LaB_6 was used for correction of geometrical parameters and subsequent integration of Debye–Scherrer rings into 2θ patterns. SXRD data are reported as a function of the scattering vector $Q = 4\pi \sin(\theta)/\lambda$ and assessment of structural information was made using MAUD, a diffraction analysis software based on the Rietveld method with focus on materials science studies [20]. Structural information of the Li–Mg–N–H were taken from literature: α- and β-$Li_2Mg(NH)_2$ [15], $Li_2Mg_2(NH)_3$ [21], LiMgN [22], $LiNH_2$, $Mg(NH_2)_2$ [23], and MgNH [24].

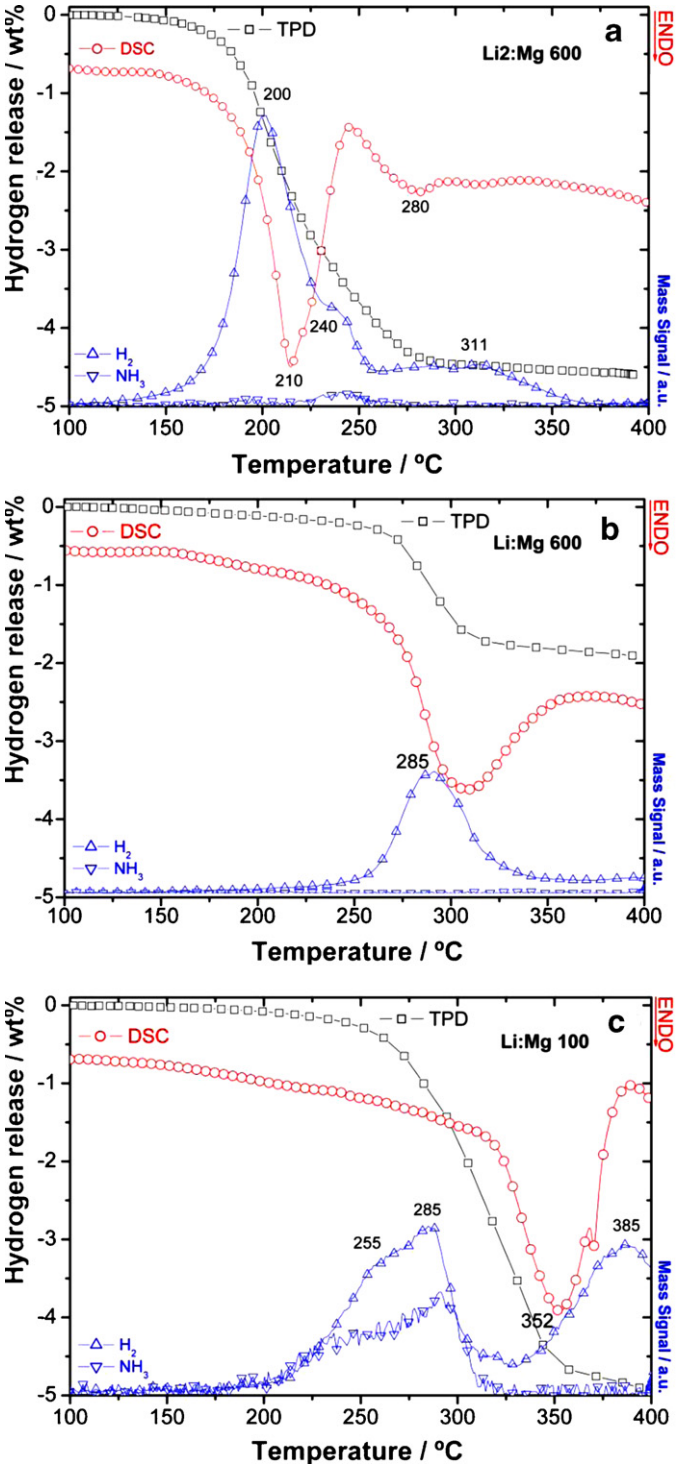

Fig. 2. MS, TPD and DSC profiles relative to samples: Li2:Mg 600 (a), Li:Mg 600 (b), and Li:Mg 100 (c).

3. Results and discussions

The SXRD patterns taken at room temperature for samples as ball milled with different rotation speeds and Li:Mg ratios are illustrated in Fig. 1. Thermal analysis (MS, TPD and DSC) used as a support for understanding the structural evolution, in terms of gas species, quantity, and reaction heat associated to each phenomenon

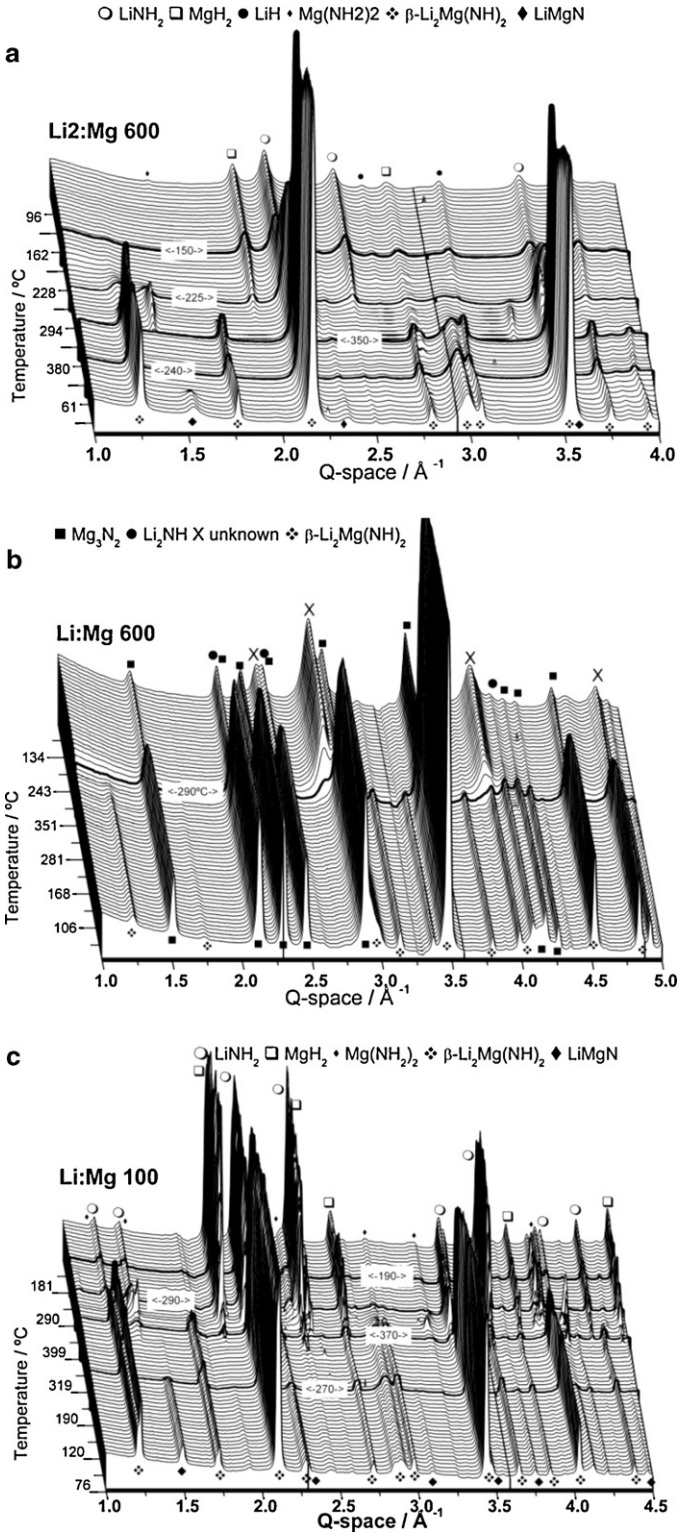

Fig. 3. SXRD as a function of temperature of samples: Li2:Mg 600 (a), Li:Mg 600 (b), and Li:Mg 100 (c).

Table 1
Structural information related to $LiNH_2/MgH_2$ samples as ball milled (BM) and after heat treatment (HT). After BM traces of MgO (<5 wt%) have been found [Rw < 6%].

Phase	Space group	Cell parameters (Å)			Crystallite size (nm)		Phases quantity (wt%)	
		a	*b*	*c*	BM	HT	BM	HT
Li2:Mg 600								
$LiNH_2$	*I*4	5.105	–	10.173	50	–	63	–
MgH_2	*P*42/*mnm*	4.521	–	3.023	30	–	15	–
LiH	*Fm*3*m*	4.109	–	–	90	–	13	–
$Mg(NH_2)_2$	*I*41/*acdz*	10.375	–	20.062	50	–	8	–
β-$Li_2Mg(NH)_2$	*P*43*m*	5.043	–	–	–	100	–	88
LiMgN	*Pnma*	7.129	3.513	5.082	–	90	–	7
Li:Mg 600								
Li_2NH	*Fm*3*m*	5.096	–	–	90	–	–	–
Mg_3N_2	*Ia*3	5.124	–	–	70	100	–	73
X (Unknown)	*Fm*3*m*	4.5	–	–	30	–	–	–
β-$Li_2Mg(NH)_2$	*Iba*2	10.220	–	–	–	90	–	24
Li:Mg 100								
$LiNH_2$	*I*4	5.185	–	10.554	100	–	57	–
MgH_2	*P*42/*mnm*	4.641	–	3.106	120	–	37	–
α-$Li_2Mg(NH)_2$	*Iba*2	9.787	4.993	5.201	100	–	3	–
β-$Li_2Mg(NH)_2$	*P*43*m*	5.179			–	100	–	95
LiMgN	*Pnma*	7.362	3.466	5.169	–	90	–	5

are shown in Fig. 2. Finally, in-situ SXRD as a function of temperature of the three samples are shown in Fig. 3. Patterns taken at room temperature for various samples after in-situ SXRD analysis are also reported in Fig. 1. Rietveld refinement results of the three samples before and after heat treatment are listed in Table 1. In order to better elucidate the results, this section is divided and discussed by sample.

3.1. Li2:Mg 600 rpm

Initial SXRD pattern of Li2:Mg milled at 600 rpm (Fig. 1a) presents very broad peaks of the initial phases $LiNH_2$ and MgH_2, together with a small amount of $Mg(NH_2)_2$ and LiH phases (Table 1) induced by ball milling preparation. As observed by previous work in the Li2:Mg system [16,17], ball milling can indeed promote the metathesis reaction but also partial dehydrogenation, depending on the milling times. TPD-MS-DSC thermal analyses for the sample Li2:Mg 600 (Fig. 2a) are in good agreement with each other, with a small shift of 10 °C of the main hydrogen desorption peak. Hydrogen release starting at 125 °C in the MS data matches with the decay of MgH_2 and $LiNH_2$ peaks and background intensities with subsequent appearance at 200 °C of a new phase (Fig. 3a). This phase may be signed to the $Mg(NH_2)_2$ phase, and such transformation is observed to precede the formation of polymorph α-$Li_2Mg(NH)_2$ and at 350 °C is followed by its transformation into β-$Li_2Mg(NH)_2$. The observed hydrogen release of 4.5 wt% (Fig. 2a) corresponds to the formation of $Li_2Mg(NH)_2$ phase during decomposition under helium pressure, but also under vacuum conditions [15] and isothermal measurements [2,3] for the Li2:Mg system. During cooling, a decrease of the peaks of β-$Li_2Mg(NH)_2$ and the appearance of peaks of LiMgN are observed at about 240°C, close to the calculated value for the complete decomposition reaction of $LiNH_2 + MgH_2$ mixture [6].

3.2. Li:Mg 600 rpm

SXRD pattern of the sample Li:Mg milled at 600 rpm (Fig. 1b) presents broad diffraction peaks due a microstructure refinement during ball milling. There are no reflections left of the starting materials $LiNH_2$ or MgH_2. Previous studies of the influence of ball milling conditions in the Li:Mg system pointed to the possible formation of $Mg(NH_2)_2$ or MgNH phases [18,19]. In this work, the Li:Mg sample ball milled for 12 h at 600 rpm presented the signature of Li_2NH and Mg_3N_2 phases. In addition, an unknown phase not identified with any one in the ICSD available database was observed. This unknown (X) phase can be indexed as a face-centered cubic cell with space group *Fm*3*m* and a lattice constant of $a_0 \sim 4.5$ Å. A list of the Bragg reflections indices and interplanar distance is reported in Table 2. A γ-$Li_2Mg(NH)_2$ phase, observed for the Li2:Mg system at temperatures higher than 450 °C, has been indexed with a similar structure ($a_0 \sim 5$ Å) in a previous work [15]. In addition, a recent work [25] on the $LiNH_2$-CaH_2 system reported the formation of the cubic CaNH phase after ball milling. Thermal analysis of the Li:Mg 600 (Fig. 2b), resulted in a single step release of 2 wt% H_2 at about 285 °C, presenting an endothermic character. For this sample, thermal profile by the three different techniques (MS-TPD-DSC) are in good agreement. In-situ SXRD analysis (Fig. 3b) of Li:Mg 600 sample confirms a single desorption event at about 285 °C under 3 atm He, where the diffraction peaks of both Li_2NH and unknown (X) phase decrease, together with the appearance of β-$Li_2Mg(NH)_2$ phase and the increase of the Mg_3N_2 phase. Even though it is known only an hexagonal MgNH phase [24] this reaction step supports the presence of a MgNH compound as the unknown (X) phase. This event may open space for the occurrence of a cubic metastable MgNH in certain conditions, with a structure similar to that of the CaNH phase. It is worth noting that the decomposition of the unknown phase is independent on the reaction conditions, as evidenced by the similarity of the results obtained from the DSC, MS, TPD and SXRD analysis.

3.3. Li:Mg 100 rpm

The SXRD pattern of sample Li:Mg 100 (Fig. 1c) consists mainly of sharp peaks of the parent phases, with no apparent microstructural refinement resulting from ball milling procedure. However, the presence of a small fraction of α-$Li_2Mg(NH)_2$ was considered for Rietveld refinement (Table 1). For the Li:Mg system, infrared

Table 2
Bragg reflection indices and interplanar distance of the X phase (*Fm*3*m*, $a \sim 4.5$ Å) identified in the as ball milled Li:Mg 600 sample.

#	*hkl*	d_{hkl} (Å)
1	1 1 1	2.61
2	2 0 0	2.25
3	2 2 0	1.59
4	3 1 1	1.36

spectroscopy analysis showed the formation of $Li_2Mg(NH)_2$ by ball milling [20]. In addition, recent thermodynamic studies have put in evidence the higher stability of $Li_2Mg(NH)_2$ compared to $LiNH_2$ [26]. Thermal analysis of sample Li:Mg 100 (Fig. 2c) presents two distinct peaks of hydrogen release at around 270 °C and 380 °C, the former one accompanied by ammonia release. For this sample, signals of MS and DSC present distinct profiles and this difference is not completely clear yet. SXRD pattern development (Fig. 3c) shows progressive decomposition of $LiNH_2$ and MgH_2 into $Mg(NH_2)_2$ and mixed imide $Li_2Mg_2(NH)_3$ [22]. This reaction step, involving a multi-phase equilibria and mediate by both hydrogen and ammonia release (Fig. 2c), proceeds until the formation, at around 370 °C, of β-$Li_2Mg(NH)_2$, in agreement with the results obtained for the Li2:Mg system. During cooling, the SXRD analysis evidenced the appearance of diffraction peaks of LiMgN phase in the same temperature range predicted by DFT calculations [9].

4. Conclusions

Depending on the stoichiometry and ball milling conditions, $LiNH_2$–MgH_2 samples showed distinct initial phases and thermal desorption profiles. High energy ball milling of the Li2:Mg sample at 600 rpm initiated a metathesis reaction to $Mg(NH_2)_2$ and LiH, while identical milling conditions for the Li:Mg sample apparently enabled quite different reactions, leading to the formation of new phases. Considering the low H_2 desorption (2 wt%) of sample Li:Mg 600 during heating and the appearance of Li_2NH and Mg_3N_2 phases already after milling, it is likely that the material partially decomposed already during milling. Still, hydrogen release for Li2:Mg 600 and Li:Mg 600 samples started at 125 °C and 225 °C, respectively. On the other hand, Li:Mg 100 sample shows at 175 °C a simultaneous release of hydrogen and ammonia. In-situ synchrotron X-ray diffraction analysis showed the related solid state transformations. The broadening of the diffraction peaks and the structural similarities of the involved crystal phases made a careful quantitative analysis rather difficult. The results presented above underline the complexity of the Li–Mg–N–H hydrogen storage systems and its crucial dependence of the materials performance on stoichiometry and milling conditions.

Acknowledgments

This study was supported by the European Commission under FP6 project: COSY (MC-RTN-2006-035366). The authors thank the ESRF for the provision of beam time.

References

[1] P. Chen, Z. Xiong, J. Luo, J. Lin, K.L. Tan, Nature 420 (2002) 302–304.
[2] W. Luo, J. Alloys Compd. 381 (2004) 284–287.
[3] Z. Xiong, G. Wu, J. Hu, P. Cheng, Adv. Mater. 16 (2004) 1522–1525.
[4] H. Leng, T. Ichikawa, S. Hino, N. Hanada, S. Isobe, H. Fujii, J. Phys. Chem. B 108 (2004) 8763–8765.
[5] Y. Nakamori, G. Kitahara, K. Miwa, N. Ohba, T. Noritake, S. Towata, S. Orimo, J. Alloys Compd. 404–406 (2005) 396–398.
[6] S.V. Alapati, J.K. Johnson, D.S. Sholl, J. Phys. Chem. B 110 (2006) 8769–8776.
[7] A.R. Akbarzadeh, V. Ozolins, C. Wolverton, Adv. Mater. 19 (2007) 3233–3239.
[8] J. Lu, Z.Z. Fang, Y.J. Choi, H.Y. Sohn, J. Phys. Chem. C 111 (2007) 12129–12134.
[9] Y. Liu, K. Zhong, M. Gao, J. Wang, H. Pan, Q. Wang, Chem. Mater. 20 (2008) 3521–3527.
[10] W. Osborn, T. Markmaitree, L. Shaw, J. Power Sources 172 (2007) 376–378.
[11] H. Leng, T. Ichikawa, H. Fujii, J. Phys. Chem. B 110 (2006) 12964–12968.
[12] W. Lohstroh, M. Fichtner, J. Alloys Compd. 446–447 (2007) 332–335.
[13] M. Aoki, T. Noritake, G. Kitahara, Y. Nakamori, S. Towata, S. Orino, J. Alloys Compd. 428 (2007) 307–311.
[14] Y. Nakamura, S. Hino, T. Ichikawa, H. Fujii, J.H. Brinks, B.C. Hauback, J. Alloys Compd. 457 (2008) 362–367.
[15] J. Rijssenbeek, Y. Gao, J. Hanson, Q. Huang, C. Jones, B. Toby, J. Alloys Compd. 454 (2008) 233–244.
[16] S. Barison, F. Agresti, S. Lo Russo, A. Maddalena, P. Palade, G. Principi, G. Torzo, J. Alloys Compd. 459 (2008) 343–347.
[17] R. Shahi, T.P. Yadav, M.A. Shaz, O.N. Srivastava, J. Alloys Compd. 33 (2008) 6188–6194.
[18] C. Liang, Y. Liu, K. Luo, B. Li, M. Gao, H. Pan, Q. Wang, Chem. Eur. J. 16 (2010) 693–702.
[19] J. Lu, Y.J. Choi, Z.Z. Fang, H.Y. Sohn, J. Power Sources 195 (2010) 1992–1997.
[20] L. Lutterotti, S. Matthies, H.-R. Wenk, A.J. Schulz, J. Richardon, J. Appl. Phys. 81 (1997) 594–600, MAUD is available at http://www.ing.unitn.it/~maud.
[21] E. Weidner, F. Dolci, J. Hu, W. Lohstroh, T. Hansen, D.J. Bull, M. Fichtner, J. Phys. Chem. C 113 (2009) 15772–15777.
[22] A. Bailey, P. Hubberstey, R.W. Hughes, C. Ritter, D.H. Gregory, Chem. Mater. 22 (2010) 3174–3182.
[23] M.H. Sorby, Y. Nakamura, H.W. Brinks, T. Ichikawa, S. Hino, H. Fujii, J. Alloys Compd. 428 (2007) 297–301.
[24] O. Dolotko, H. Zhang, S. Li, P. Jena, V. Pecharsky, J. Alloys Compd. 506 (2010) 224–230.
[25] J. Jacobs, Z. Anorg, Allg. Chem. 370 (1969) 254.
[26] F. Xu, L.X. Sun, P. Chen, Y.N. Qi, J. Zhang, J.N. Zhao, Y.F. Liu, L. Zhang, Z. Cao, D.W. Yang, J.L. Zeng, Y. Du, J. Therm. Anal. Calorim. 100 (2009) 401–406.